Target Detection Using An AOTF 1 Iyperspectral Imager

L.J. Cheng, J.C. Mahoney, and G.F. Reyes
Jet Propulsion Laboratory
California Institute of Technology
Pasadena, CA 91109

H.R. Suiter
Coastal Systems Station
Naval Surface Warfare Center
Panama City, FL 32407-7001

ABSTRACT

This paper reports results of a recent field experiment using a prototype system to evaluate the acousto-optic tunable filter polarimetric hyperspectral imaging technology for target detection applicat ions.

1. INTI<ODUCTION

Acousto-optic tunable filter (AOTF) is a special acousto-optic device invented by 1. C. Chang[1]. Functionally, AOTF is a real-time programmable, high-resolution spectral bandpass filter with polarization beam splitting capability, With proper optics and focal plane arrays, one can build a polarimetric hyperspectral imaging (PHI) system capable of measuring spatial, spectral, and polarization characteristics of a target with a single instrument.

]n the past, we developed two laboratory breadboard systems and investigated the technology potential for space exploration applications.[2,3] One operated in a visble/near-infrared wavelength range and the other in the short-wave infrared range. Recently, we developed an AOTF-PHI prototype system operating in a wavelength range of 0.48-0.75 microns[5] and have done a number of outdoor field experiments for evaluating the system perfqrmnacé,)incl uding one at Ft. Huachuca, AZ during an Army exercise.[6,7] This paper reports a field observation on a group of small targets in different outdoor surroundings at JPL using the prototype system.

2. OBSERVATION CONDITION

The targets included inactive land mines, cement blocks, and plastic pipes. The targets were placed in three different surroundings, i.e. an iceplant field (ice), a bare ground with a "white" trailer nearby (dirt), and an open steel frame about 1 meter from the ground (big). The iceplant field was a mixture of healthy and dead iceplants with uneven distribution, providing a background of spectral variation. Some targets were placed on the top of the iceplant and some were pushed into the iceplant field so that only a small part of the target was visible. This arrangement did provide an interesting challenge for testing the instrument. A Halon plate of unity reflectance over the instrument wavelength range was also placed in the scene for intensity normalization.

in the 'ice' and 'dirt' runs, the distance between the target area and the instrument was about 400 meters. The instrument was on the top of a small hill and looked at the area with a downward angle of about 30 degrees and directed at 210 degrees south, The 'ice' run was carried out at the noon and the 'dirt' run was around 3 PM. in the 'big' run, the instrument directed at 270 degrees west and the time was 10 AM. The targets were located about 40 meter away from the instrument, Both were on a small plateau of the hill. The weather was sunny with typical Los Angles basin smog in July.

After the observation, the data were converted into the form of image cubes. Each run had two spectral image cubes with polarization orient ations perpendicular (V) and parallel (H) to the horizon. Spectra] derivative and polarization image cubes were also formed for more detailed examinations.

The processed data did provide interesting and valuable information on spectral and polarization characteristics of targets and effects of surroundings on measured signatures. A set of selected results is given in this paper for illustrating technology potentials and issues to bc investigated.

3. EXPERIMENTAL RESULTS

3.1 Spectral Mixing

Spectral mixing is a very important issue in remote sensing with hyperspectral instruments. The scattering of the scattered light from the surrounding objects will be observed as a part of the total photon flux from the target, The measured spectrum of the target is a weighted sum of its own spectrum and those of its surrounding objects, This spectral mixing problem is expected to become more serious for small targets, especially for those partially buried in the iceplant field.

Figure 1 and 2 gives observed spectra of a dark green round metallic mine and a green square plastic mine, respectively, with H and V polarization orientations in the three different surrounding conditions, The data in the figures show clearly that the measured spectra of the mines were influenced significantly by the spectral characteristics of its surroundings, Significant differences in intensity and spectral structure between H and V polarization data were also observed. In addition, each spectrum shows a considerable amount of background light over the measured wavelength range. This is due to light scattering at aerosol and particles in air that also relates to solar radiance and total reflectance in the surrounding. Also the scattering produces polarization effects in solar light as the way observed here.

The spectra in Figure 1 provide the following observations:

* The green paint applied on the metallic mine did not have any feature resembling vegetation chlorophyll red edge absorption around 0.7 micron ('big', H);
* Small influence by the presence of vegetation nearby as indicated by a small signal rise around 0.7 micron ('big', V);
* Spectrum of the same mine in the iceplant field being similar to that of vegetation, duc to the fact that the target was pushed in the iceplant field resulting high spectral contamination due to the surrounding ('ice', H&V);
* Strong spectral mixing from the 'white' trailer wall ('dirt', H&V); and
* Measurable differences in intensity and spectrum taken at H and V polarization orientations ('ice', 'big', and 'dirt'),

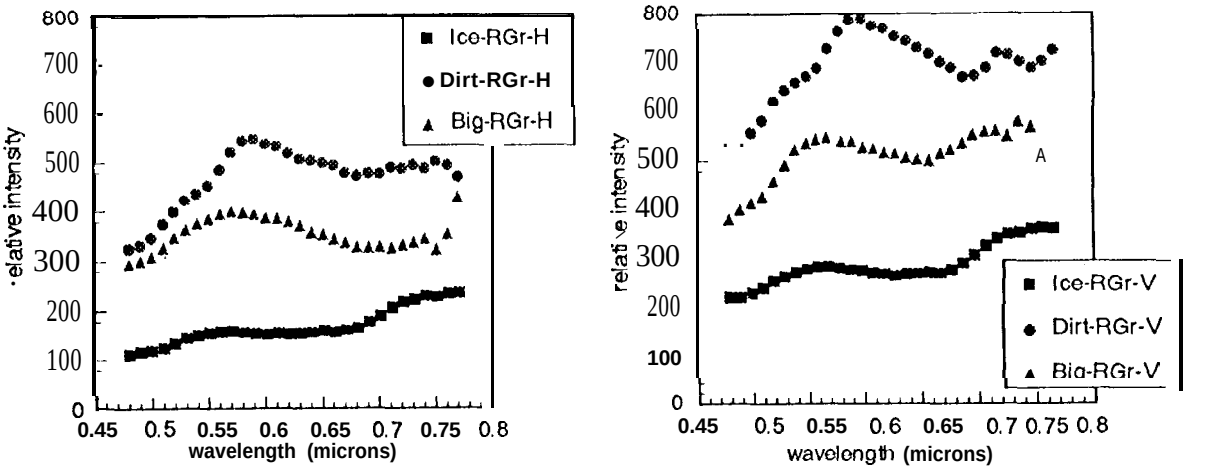

Figure 1. Observed spectra of a dark green round metallic mine in three different surroundings: iceplant filed (ice); bare (dirt) ground field near a white trailer; and on-a-steel-rail about 1 meter high from the ground and data was taken at a close distance(big).

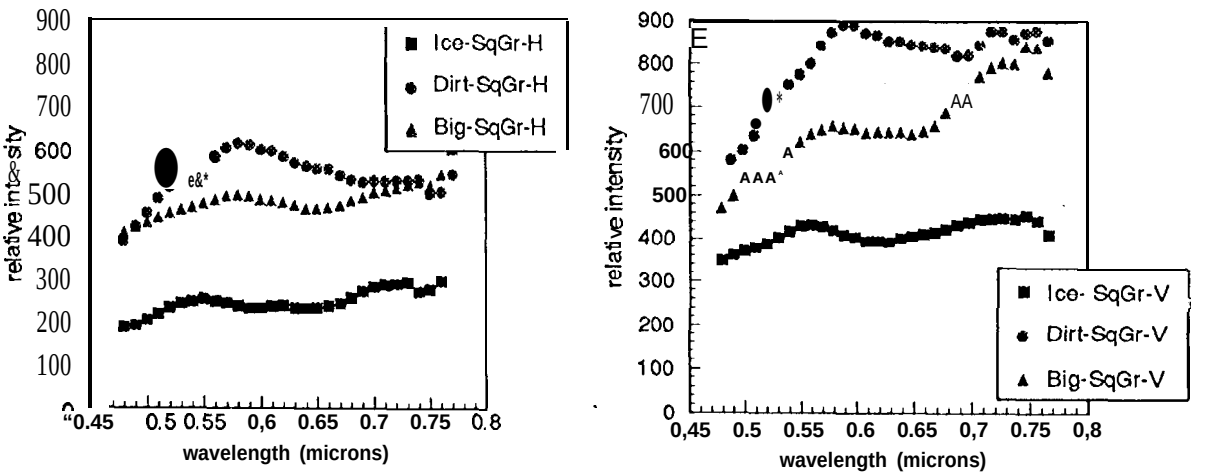

Figure 2. Observed spectra of a green square plastic mine in the same surroundings stated in Figure 1,

Figure 2 gives observed spectra of a square green plastic mine in the three same environments. Wc observed the following:

* The influence from the iceplant was small, because the plastic mine was 'placed on the top of the iceplant ('ice', H&V);
* Observable spectral mixing from surrounding vegetation ('big', H&V);
* Strong spectrum mixing duc to the 'white' trailer ('dirt', H&V); and
* Similar polarization effects observed ('ice', 'dirt', and 'big').

From the above-stated observations, it may be concluded that spectrum mixing duc to surrounding objects is an unavoidable event. However, there are ways to separate individual components from the

observed spectral data, if spectra of individual components arc known. There are a number of methods available. They arc common] y used in spectroscopy.7

3.2 Spectra] and Polarimetric Images

This section gives an illustration of important features in spectral and polarization images of the iceplant field with manmade targets,

Figure 3 gives spectral and spectral derivative images of a scene of the iceplant field taken at 0.72 micron, The scene contains two dark green round met allic mines, two light green square plastic mines, a cement block, and a white plastic pipe. In addition, there arc living and dead the iceplant. In the lower part of the figure, there is a sketch for indicating approximately the location of these man-made targets, Except the green square plastic mine A, all the mines were pushed in the iceplant with a portion being visible,

Since the chlorophyll red absorption edge occurs around 0.7 micron, vegetation is more reflective at 0.72 micron and spectral derivative signal becomes very high. These two phenomena can be used to distinguish green manmade targets from green vegetation.

In the spectral images, all targets were observable but not clearly. Target B appeared to be a black spot because a hole in the ice plant was formed when the target was pushed in the iceplant field. In the spectral derivative images, the vegetation became much brighter because of the rapid change in chlorophyll absorption with wavelength. Therefore, all targets and dead plants became dark in comparison with health the iceplant.

In the lower right part of the spectral image, the iceplant had yellow flower buds appearing to be brighter in comparison with normal the iceplant. The yellow flower bud spectrum does not have the dominating signal of chlorophyll. Therefore, this area appeared to be darker in the spectral derivative image.

A 45-degree-tilt darker strip toward the upright corner of the spectral image contained a mixture of health, unhealthy, and dead iceplants. Because of loss of chlorophyll, the dead the iceplant were black dots in the both spectral and spectral derivative images. In addition, the cement F and the white pipe E were observable because they are bright in comparison with their surroundings. It is difficult to observe the mines, A, C, and D, because lack of proper contrast in the image.

In the spectral derivative pictures, the appearance of the images changed considerably. The wavelength of 0.72 micron is still in the chlorophyll red edge transition range, healthy vegetation has high spectral derivative signals, showing up as being bright. This derivative approach provides a good contrast for the vegetation with respect to the others. The dead plants (in the center of the image) arc very dark, because they lost the chlorophyll. All others, including mines, cement block, plastic pipe, also appear to be dark, Remember that dark areas could be vegetation in the shallow. They arc generally random in shape, whereas the man-made objects often have some regular geometry, This regularity was lost when the mines were partially hidden behind the iceplant.

Spectral Images

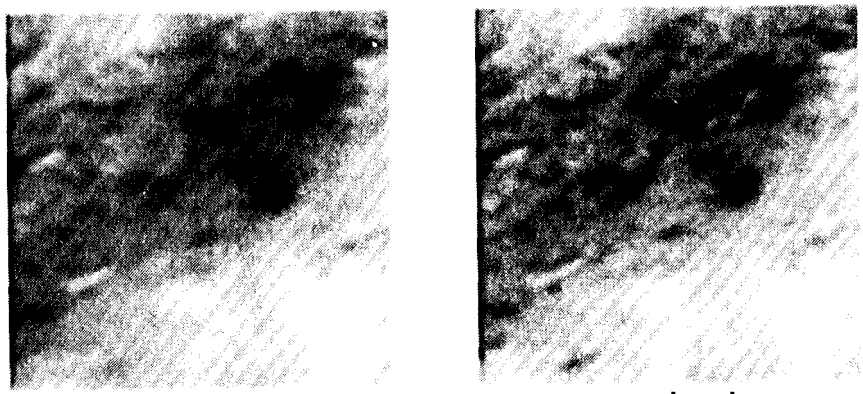

horizontal vertical

Spectral Derivative Images

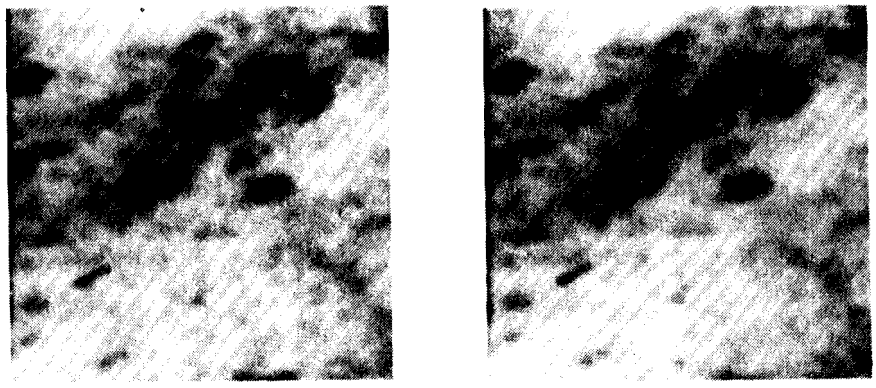

horizontal vertical

Wavelength = **0.72** micron

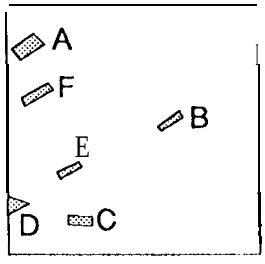

A &D: Green square plastic mines
B & C: Green round metallic mines
E: white plastic pipe
F: Cement block

Figure 3. Spectral and spectral derivative images of a scene taken at 0.72 micron with H and V polarization. A sketch indicates the location of targets.

It is noted that the green mine B was very dark with a shape different from a single mine pattern. Actually, the black shape contains the whole disturbance created by the action of pushing the mine into the iceplant field. This disturbance created a hole in the iceplant filed at the upside of the mine. The combinat ion of the two formed a dark 'PACM AN' pattern as observed.

Figure 4 gives an image of the same area at 0.55 micron. Square mine A, cement block F, and white pipe E appear to be very bright. The long shape pattern of green mine B is clearly observable. Also the spectral images provide more topographical features than the near-infrared ones. In the spectral derivative images, the appearance of square mine A, cement block F, and pipe E arc drastically different from that in the spectral images.

Polarization is an important parameter in remote sensing. Its applications have not been well developed yet, The AOTF instrument is capable of providing images of two polarization orientations perpendicular to each other, Figure 5 gives images of another iceplant scene. There are two green mines with smooth surfaces, A and B, a cement block C, and Halon plates D and E as illustrated at the lower part of the figure.

The spectral image on the left, taken with H polarization, shows a two connected bright dots tilt in 45 degrees, that is the cement block C. The two mines A and B were not visible in the horizontally polarized image. They are clearly visible as two bright dots in the image of V polarization, located at upper and lower sides of the cement block. The bright dots could be due to specular reflection from the mine surface. Three polarization images in the middle of Figure 5 are formed using the formula of polarization $P = (I_v-I_h)/(I_v+I_h)$, where J, and I_h are intensities of vertically and horizontally polarized light at each pixel, The two mines are bright in the polarization images. It is interested to note that both the cement block and HaIon targets are dark with respect to that of vegetation at wavelengths of 0.62 and 0.63 microns, However, at 0.64 micron, these objects suddenly become brighter with the signals equivalent to that of vegetation. The physical mechanism creating the change is not known, A possible explanation is given in the next paragraph.

Up to date, we have only inspected visually all the image cubes created by the data. We have seen the complexity of the target signature change with wavelength and polarization, It is known that the maximum absorption of chlorophyll occurs around 0.65 micron, The spectral derivative signal of chlorophyll at the wavelength is theoretically zero. This provides opportunities to observe targets that arc not related to vegetation. At this wavelength range, our data did provide better images of the mines C and D as shown in Figures 3 and 4. The appearance change in polarization signatures of the cement block and the Halon plate at 0,64 micron discussed in the previous paragraph could be related to the effect.

4. CONCLUSION

Our field observation results do illustrate the powerful capability of the AOTF-PHI technology for target detection in the different surroundings, The results also show the complexity of the outdoor field observation environment. In order to take the advantage of PHI, there is a need to understand the fundamental physical phenomena involved in the observation.

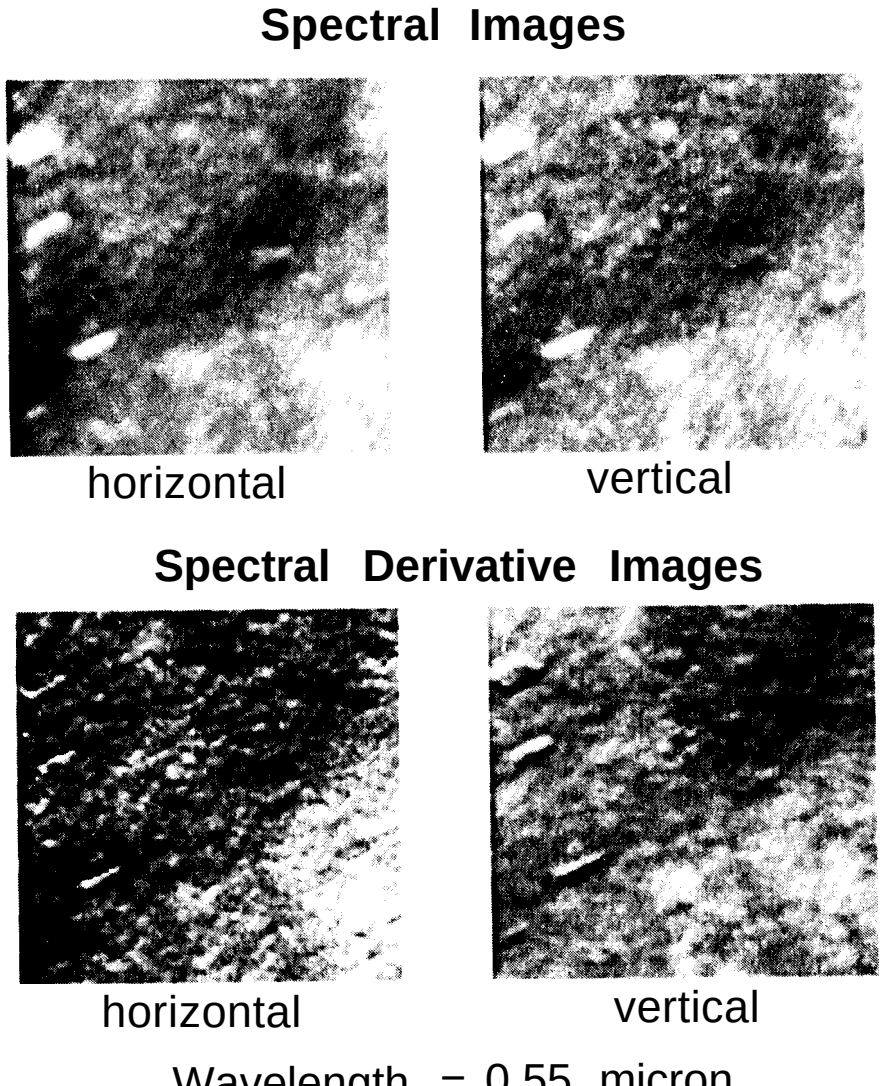

Figure 4. Spectral and spectral derivative images of the same scene in Figure 3, but taken at 0.55 micron.

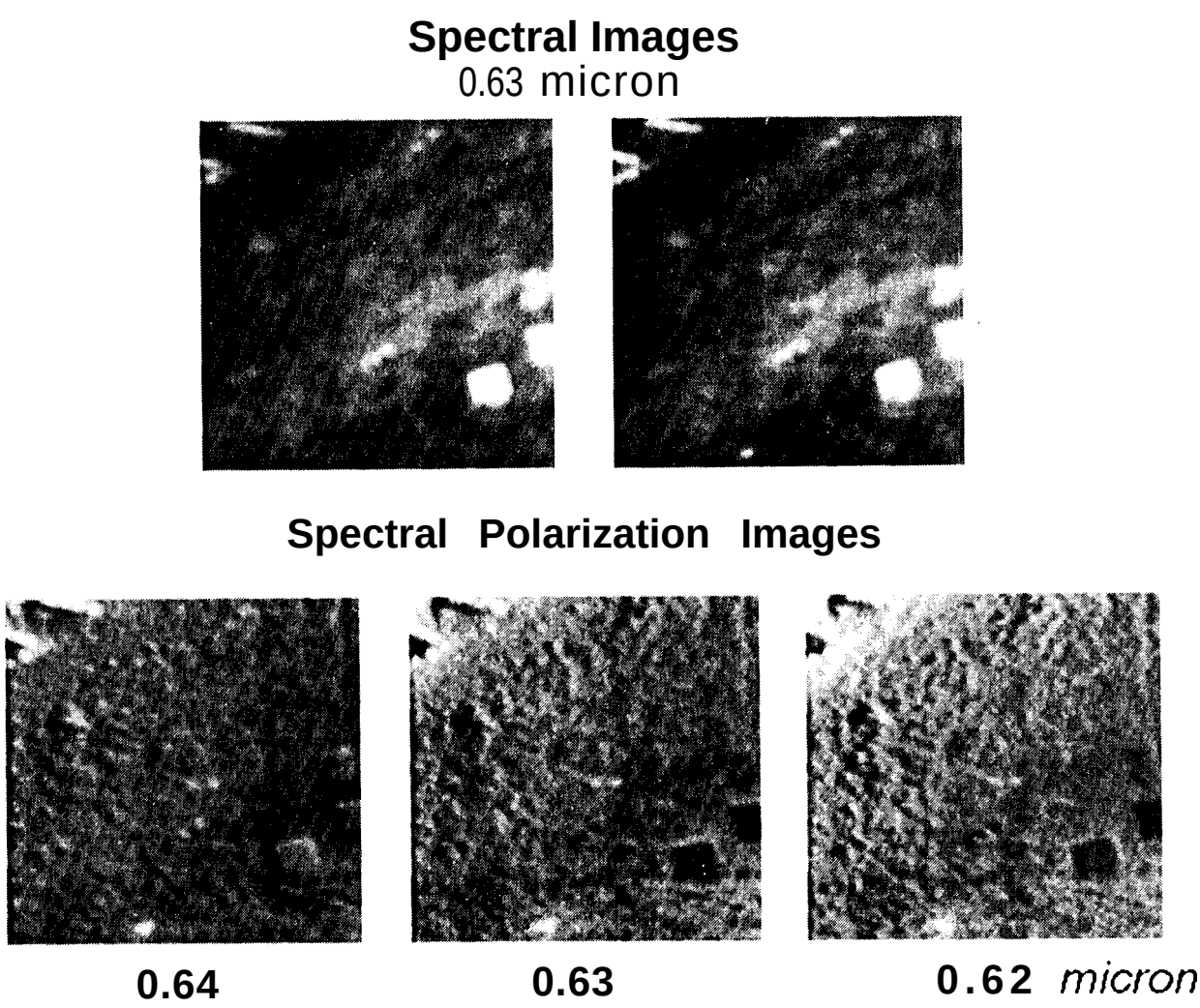

Figure 5. Spectral images of another scene taken at 0.63 microns and three spectral polarization images taken at 0.62, 0.63, and 0.64 mocrons. A sketch indicates the location of targets,

S. ACKNOWLEDGMENT

The research described in this paper was performed by the Center for Space Microelectronics Technology, Jet Propulsion Laboratory, California Institute of Technology, and was jointly sponsored by the Naval Surface Warfare Center and National Aeronautics and Space Administration, Office of Advanced Concepts and Technology.

6. REFERENCES

1. I.C. Chang, "Noncollinear Acousto-Optic Filter with Large Angle Aperture", Appl. Phys. Lett., Vol. 25, p.370 (1974).

2. Tien-Hsin Chao, Jeffrey Yu, George Reyes, David Rider and Li-Jen Cheng, "Acousto-Optic Tunable imaging Spectrometers", Proceedings of 1991 International Geoscience and Remote Sensing Sympoium, Helsinki, Espoo, FINLAND, June, 1991 (IEEE 91 CH297 1-O), p. 585.

3. Li-Jen Cheng, Tien-Hsin Chao, and George Reyes, "Acousto-Optic Tunable Filter Multispectral imaging System", AIAA Space Programs and Technologies Conference, March 24-27, 1992, paper 110.92-1439.

4. Li-Jen Cheng, Tien-Hsin Chao, Mack Dowdy, Clayton LaBar, Colin Mahoney, George Reyes, and Ken Bergman, "Multispectral Imaging Systems Using Acousto-Optic Tunable Filter" , in "Infrared and Millimeter Wave Engineering" , SPIE Proceedings Vol. 1874, p. 224 (1993),

5. Li-Jen Cheng, Mike Hamilton, Colin Mahoney, and George Reyes, "Field Observations Using An AOTF Polarimetric Imaging Spectrometer", in " Summaries of the Fourth Annual JPL Airborne Geoscience Workshop, October 25-29, 1993", edited by R.O. Green, JPL Publication 93-26, Vol. 1, p.19, 1993.

6. Li-Jen Cheng, Mike Hamilton, Colin Mahoney, and George Reyes, "Analysis of AOTF Hyperspectral Imagery", To be published in SPIE Proceedings , Vol .2231, (1994).

7. For example, S. Banerjee and D. Li, 'Interpreting Multicomponent Infrared Spectra by Derivative Minimization', Appl. Spectrosc, vol 45, p. 1047 (1991).